Research article

Soojung Kim, Hyerin Song, Heesang Ahn, Seung Won Jun, Seungchul Kim, Young Min Song, Seung Yun Yang, Chang-Seok Kim and Kyujung Kim*

3D super-resolved imaging in live cells using sub-diffractive plasmonic localization of hybrid nanopillar arrays

Abstract: Analysing dynamics of a single biomolecule using high-resolution imaging techniques has been had significant attentions to understand complex biological system. Among the many approaches, vertical nanopillar arrays in contact with the inside of cells have been reported as a one of useful imaging applications since an observation volume can be confined down to few-tens nanometre theoretically. However, the nanopillars experimentally are not able to obtain super-resolution imaging because their evanescent waves generate a high optical loss and a low signal-to-noise ratio. Also, conventional nanopillars have a limitation to yield 3D information because they do not concern field localization in z-axis. Here, we developed novel hybrid nanopillar arrays (HNPs) that consist of SiO_2 nanopillars terminated with gold nanodisks, allowing extreme light localization. The electromagnetic field profiles of HNPs are obtained through simulations and imaging resolution of cell membrane and biomolecules in living cells are tested using one-photon and 3D multiphoton fluorescence microscopy, respectively. Consequently, HNPs present approximately 25 times enhanced intensity compared to controls and obtained an axial and lateral resolution of 110 and 210 nm of the intensities of fluorophores conjugated with biomolecules transported in living cells. These structures can be a great platform to analyse complex intracellular environment.

Keywords: hybrid nanopillar arrays; plasmon-enhanced fluorescence imaging; super-resolution imaging.

*Corresponding author: Kyujung Kim, Department of Cogno-mechatronics Engineering, Pusan National University, Busan, 46241, Republic of Korea; and Department of Optics and Mechatronics Engineering, Pusan National University, Busan, 46241, Republic of Korea, E-mail: k.kim@pusan.ac.kr. https://orcid.org/0000-0002-0913-2291
Soojung Kim, Hyerin Song, Heesang Ahn and Seung Won Jun: Department of Cogno-mechatronics Engineering, Pusan National University, Busan, 46241, Republic of Korea
Seungchul Kim and Chang-Seok Kim: Department of Cogno-mechatronics Engineering, Pusan National University, Busan, 46241, Republic of Korea; Department of Optics and Mechatronics Engineering, Pusan National University, Busan, 46241, Republic of Korea
Young Min Song: School of Electrical Engineering and Computer Science, Gwangju Institute of Science and Technology, Gwangju, 61005, Republic of Korea
Seung Yun Yang: Department of Biomaterials Science, Life and Industry Convergence Institute, Pusan National University, Miryang, 50463, Republic of Korea

1 Introduction

Exploration of the single-molecule processes of the nucleus in living cells is important for understanding complex biological systems [1–4]. Fluorescence-based technologies have been used to study the structural and dynamic properties of biological proteins, such as ion channels, receptors, and transporters [5–8]. They have become a powerful tool for understanding protein–protein interactions that represent specific information about the time trajectory of proteins that interact with other related proteins and the basic steps of the reaction mechanisms. Particularly, as the fluorescence imaging based on complex topologies of nanostructures has evolved, it has become possible to explain numerous molecular mechanisms with improvement of the lateral and axial resolution of images. Thus, accurate characterization of nanoscale specimens can be achieved [9–12].

Specifically, significant researches using nanopillar structures have been reported to observe meaningful signals in biological applications [13, 14]. Vertically standing nanopillars with high aspect ratios have great potential for the investigation of living cells with optical waveguides properties and strong adhesion to nanopillar surfaces and intracellular biological molecules [15–17]. The nanopillars affect locally curving of plasma membranes and upward bending of nuclear membrane of the cells adherent to the

nanopillar topographies [18, 19]. Thus, vertical nanopillars can potentially be used to examine the functions and activities of the cell nucleus and membranes [20, 21]. This modification induces modulation of intracellular activities, such as cell adhesion [22, 23], signal transduction [24], differentiation [25, 26], and survival [27–28].

Combined with their optical and biological capabilities, nanopillars have been confirmed to have great potential as detection probes by coupling with the biological target to maximize the signal enhancement. To perform these functions, dielectric nanopillar (DNP)s are often used due to propagating light along the axis of the cylindrical nanopillars, functioning as photonic waveguides [29–33]. However, optical loss can occur through the evanescent field on the surface of the DNPs, which spreads out over a wider area from the tip when light in the visible or infrared region is incident along the axis of the DNP array. Consequently, uncertain information is obtained from the scattered optical signal of the nanopillars with a low signal-to-background ratio for the target materials, which leads to degradation of the imaging resolution. To retain a high-resolution signal, it is necessary to amplify and concentrate the intensity of the signal and reduce the light spreading caused by scattering and the evanescent waves of the nanopillars [34–37].

To address this challenging issue, we propose hybrid plasmonic nanopillar (HNP) arrays that composed of DNPs capped with gold nanodisks functioning as plasmonic waveguides. The metallic structures make it possible to guide the localized surface plasmon (LSP) phenomenon, leading to amplification of the light intensity and sub-wavelength localization of electromagnetic energy when coupled to incoming light below the plasma frequency [38–50]. In fluorescence imaging based on nanotechnology, coupling of the fluorophores and LSP modes of plasmonic nanostructures enhances the fluorescence detection sensitivity and improves the intensity of the plasmonic-coupling-based sensing signal [51–54]. The nanopillars, composed of only gold, can improve the Lateral resistance, but it is deemed difficult to improve the z-axial resolution, as it also produces light localization on the side as well as on the tip [55]. Of the various metallic materials, we select gold as the additional nanostructure on the because gold nanostructures can be functionalized with biocompatible properties and low cytotoxicity [46, 47].

We conducted simulations of the optical distribution on hybrid nanopillar arrays (HNPs) enhancement of imaging resolution and fluorescence signal. Based on the simulations, fluorescence emission of living cells cultured on HNPs were observed to evaluate the capability of HNPs to act as a detection probe. We demonstrated enhanced lateral and axial resolution of each fluorescence signal from biomolecules transported though ligand-mediated endocytosis to the nucleus for HNP-based two-photon fluorescence imaging. Consequently, we observed that the HNPs with plasmonic hotspots enable cellular analysis with improved fluorescence brightness at the single-molecule level. Then, we verified the signal amplification and observation volume driven by HNPs to determine whether the HNPs enable analysis of the individual behaviour of biomolecules, particularly inside the nucleus, with subwavelength spatial (XYZ) resolution.

2 Results and discussion

2.1 Fabrication of HNPs

To confirm the physical interaction between the surface of HNPs and cells, Scanning electron microscopy (SEM) images were taken to verify the morphological change in the cell shape when cultured on HNPs and the structural changes of the individual HNPs in close physical contact with the cells. To easily and accurately fabrication HNPs proposed in our work, e-beam lithography and reactive ion etching systems were used. We successfully fabricated HNPs with a uniform distribution as an aligned vertical nanopillar geometry (Figure 1a). As a result of the proposed methods, the fabricated structures had arrays of vertically aligned SiO_2 nanopillars with a height of 700 nm, a diameter of 200 nm, and a period of 1 μm, covered by a gold layer with a thickness of 100 nm. The Au nanocap and SiO_2 nanopillar can be clearly observed in enlarged SEM images of SiO_2 nanopillars consisting of gold caps/films (Figure 1b). The gold caps have dimensions similar to the nanopillar diameter, as observed in the top-view SEM image of the gold caps/films on SiO_2 nanopillars (Figure 2c). To show distinct separation of Au and SiO_2 more clearly, the elemental mapping analysis of the HNPs showed relative location and elemental distribution of the gold, Si and O in the SEM image of HNPs (ESI Figure S5). For application as a probe for analysing a cell, the cell must contact the nanopillars, and the nanopillar geometry must bear the stresses under the cell adhesion and spreading around the plasma membrane of the cell. The shapes of the cells were retained with cell–nanopillar adhesion and cortical tension according to the nanopillar topography (Figure 1d). Even when the plasma membrane was tightly stretched across the nanopillar substrate, the geometry of the nanopillar arrays was not broken or crushed and remained intact with the required mechanical stability. We have shown that the vertical HNP structures meet the
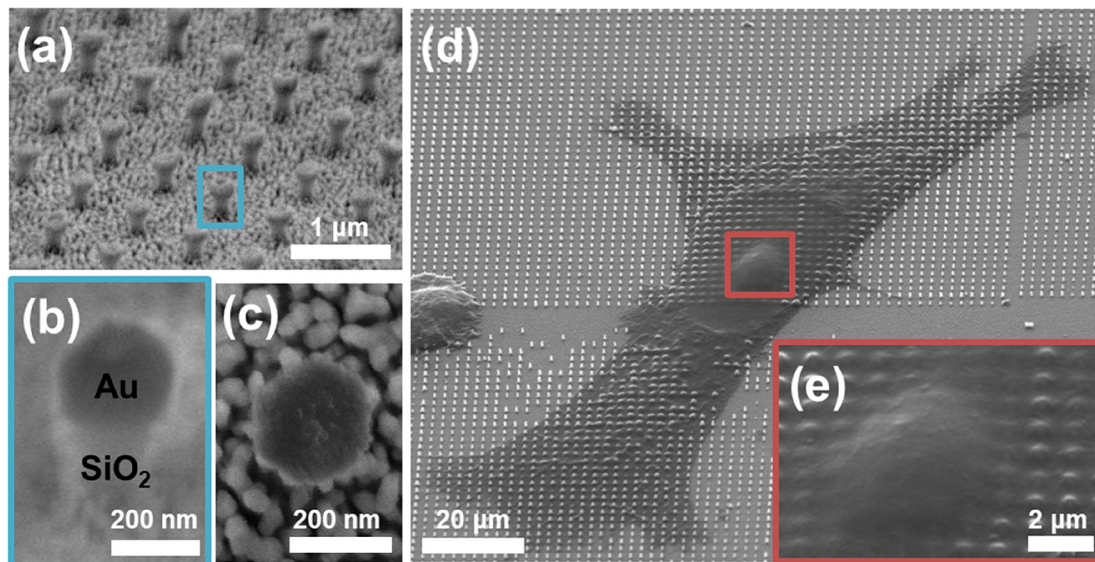
Figure 1: Scanning electron microscopy (SEM) images of vertically aligned SiO₂ nanopillars capped with gold nanodisks for intracellular fluorescence localization imaging. (a) Distribution of a highly ordered array of vertical HNPs from an SEM image showing the homogeneity in the spacing (1 μm), height (700 nm), and diameter (200 nm). (b) High-magnification SEM image showing the successfully fabricated HNP morphology with clear distinction of a SiO₂ nanopillar and a gold nanodisk. (c) Top-view of a single HNP. (d) SEM image of HeLa cells interacting with nanopillars, showing excellent adhesion of the cells to HNPs. (e) Local deformation of the nuclear membrane and plasma membrane curved due to vertical HNPs.

requirements for use as a probe to detect the localized fluorescence signal at the Au caps of HNPs at the interface of cells-HNP substrates.

2.2 Numerical calculation of electric field distributions on DNPs and HNPs

We numerically calculated the near-field distributions to analyse the field localization arising from HNPs interacting with incident light compared with DNPs. The conventional probe structures similar to those reported in [9, 11] are composed of aligned silica nanopillar arrays with a diameter of 200 nm, a height of 700 nm, and a period of 1 μm. HNPs consist of DNPs with the addition of Au nanocaps at the tips of the nanopillars and uniform Au nanofilms on the substrate of the nanopillars. The excitation waves in the simulation were 633 nm TM-polarized light incoming along the nanopillar axis. However, the measured SEM image presented in Figure 1 shows that the surface of fabricated HNPs sample has discrete formations like a layer of composed nanoparticles instead of continuous film as we designed in simulation process. Thus, we additionally performed simulation assuming the substrate layer is composed of gold nanoparticles as observed in the fabricated samples. The consequent generation of hotspots affected by uniformity of the sample substrate is presented

in Figure S6. As shown in Figure S6, the layer of composed gold nanoparticles also could provide strong hotspots at the edge of gold cap as much as that provided by the uniform gold film. As the surface uniformity insignificantly affects generating hotspots in our case and the complicated structure requires more computer resources and time during performing simulation, so the simulations were performed with uniform gold film instead of two layers of gold nanoparticles.

Light–matter interactions between the optical TM-polarized plane wave and a DNP represent the light-trapping effects on the surface of and inside the nanopillar (Figure 2a). This phenomenon is attributed to high optical energy losses, due to light scattering at the tip and side of the nanopillars (Figure 2b). Therefore, the effective measurement volume of DNP-based photonic waveguides is estimated to be greater than 150% of the nanopillar dimension, and it is difficult to distinguish single molecules from the background signal noise.

To facilitate the demonstration of essential intracellular processes at the nanoscale, it is necessary to significantly confine the illumination volume in the nanopillar probe. The proposed hybrid structures allow coupling between plasmonic fields and fluorophores, an approach that presents meaningful advantages for detecting emissions arising from nanoscale localization. Figure 2c presents the LSP modes in the gold nanodisks allow subwavelength
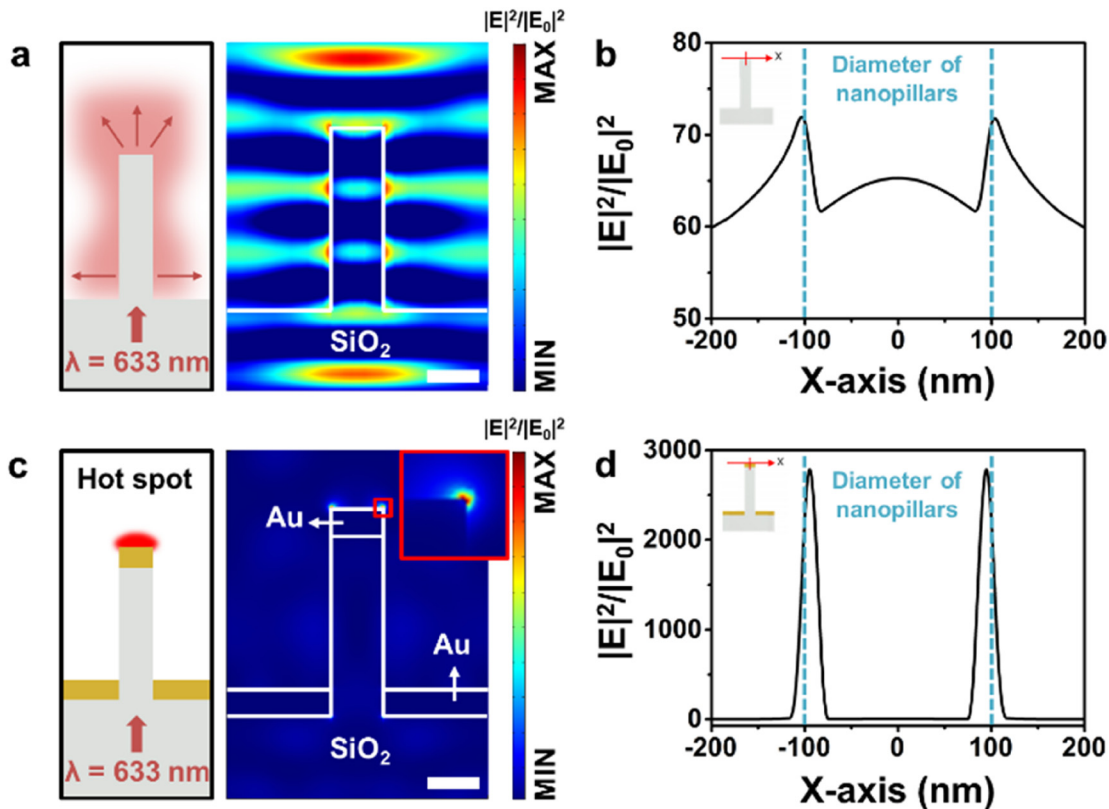
Figure 2: Normalized electric field-intensity distributions of DNPs and HNPs. (a) Schematic of subwavelength photonic waveguides and calculated electric field of the cross section of DNPs. (b) Optical X-axis line profile at the tip of DNPs. The full width at half maximum (FWHM) of the two optical maxima, as the basic result of evanescent waves, is approximately 40 nm. (c) Schematic image of plasmon concentration at the tips of HNPs. (d) Two optical hotspots at gold nanodisks representing highly concentrated electrical fields that can enhance the emission intensity of fluorophores in the nanoscale volume (Height: 700 nm, thickness of gold nanodisks and nanofilms: 100 nm, period: 1 μm, wavelength of incident light: 633 nm, scale bars: 100 nm).

localization of visible light when coupled with light signals propagating along the HNPs. They located axial position of the gold nanodisk close to the nucleus of cells by controlling the height of the nanopillars and optically propagate light as coupler to induce LSP mode at the gold nanodisks. The dark region around the nanopillars represents that the uniform gold nanofilm (GNF)s on the substrate surface near the nanopillar can considerably reduce the unwanted background noise from light scattering (transmission detection in this mode). As shown in Figure 2d, the incoming light-coupled plasmonic concentration was amplified approximately 3000 times compared to the incident light intensity. The localized light field coupled with a plasmonic cap, with a 7 nm FWHM focal spot and amplified intensity, can enhance the ability to detect the signal of a fluorescent emitter inside the nanoscale detection volume near the gold cap of the HNPs.

It has been investigated that HNPs have potential as light-concentrating probes for producing a localized fluorescence signal in the observation volume at the gold cap

by reducing the background signal by over 90% and locally modulating plasmons at the nanoscale. Therefore, the observed signal can be distinguished from the background, except along the optical path length where the nanopillars interact with the gold cap, and concentrated to a high field intensity due to the plasmonic coupling effects between the gold tip and light transmitted towards the nanopillar aperture.

2.3 Comparison and characterization of photonics and hybrid plasmonic illumination in fluorescence cell imaging

We discuss the light nanoconfinement capability of localized fluorescence probe of HNPs compared with DNPs. To analyses the light localization effects, we reduced background signals by blocking the transmission of light with the GNF on the nanopillar substrate, as illustrated in Figure 3a. Then, we

demonstrate fluorescence intensity measurements and FWHM calculations at hotspots on fluorescence images of DNPs and HNPs that HeLa cells labelled with DiD in the plasma membrane were cultured on.

On DNP structures, slight fluorescence spots are obtained in the entire area of cells excluding the nucleus, simultaneously with the fluorescence signal of the plasma membrane (Figure 3b). As mentioned above in the simulation results, this phenomenon occurred because of fluorescence signals emitted due to coupling of DiD fluorophores with evanescent waves at the surface of DNPs and wave propagation inside DNPs. This detection was

demonstrated to show that photonic nanopillars serve as noneffective detection probes. In contrast, we could observe a strong concentration of the fluorescence signals, appearing as a pixelated array, and a high signal-to-background ratio on HNPs, which work via light-emitting unit-based focussing of plasmons (Figure 3c). This phenomenon occurs as a consequence of the near-field enhancement of fluorescence signals due to coupling of light localization at the plasmonic cap with adjacent fluorophores. The result is that the individual peaks of fluorescence emissions at the tips of HNPs are clearly visible, as shown in the images. To evaluate the
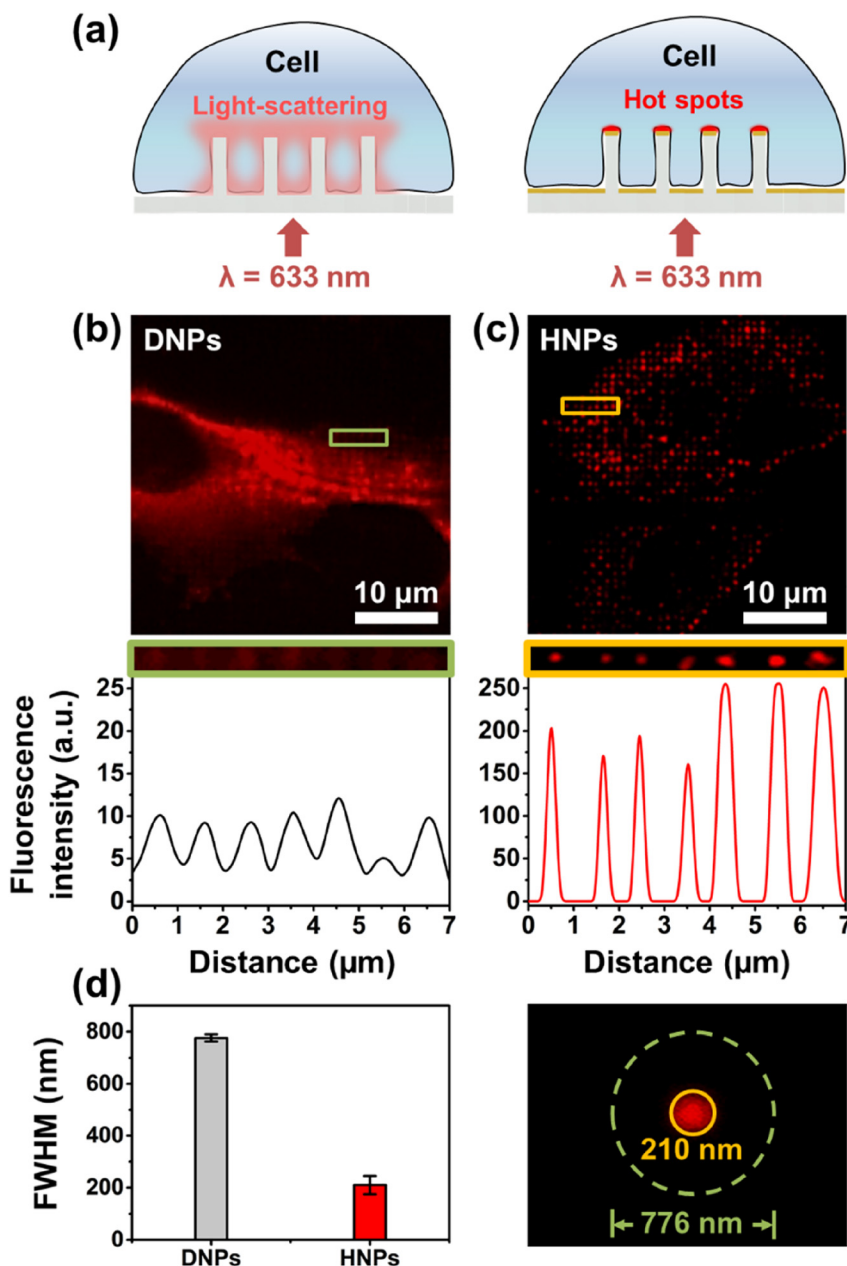
Figure 3: Measurement of fluorescence emission coupled with evanescent fields on DNPs and plasmon hot-spots on HNPs using one-photon fluorescence microscopy. (a) Schematic illumination of optical fields obtained by photonic waveguides on DNPs (left) and by plasmon focusing at the gold caps of HNPs (right). (b) Fluorescence images of HeLa cells cultured on and collected fluorescence intensity profile of zoomed-in fluorescent spot arrays with labelled cells. (c) HNP-concentrated fluorescence images, which exploit pixelated fluorescent point arrays at the plasmonic caps of HNPs that achieve emission spectra with high signal-to-background ratio and enhanced signal intensity. (d) Fluorescence FWHM comparison of individual fluorescent spots illuminated by DNPs and HNPs.

observation volumes of DNPs and HNPs as localized fluorescent probes, we quantified the distribution of the fluorescence intensities of peaks that appeared at the locations of DNPs and HNPs in the fluorescence images. The fluorescence emission profile surrounding the DNP arrays indicated that the normalized intensities at the tips of DNPs were approximately twice that in the area in the vicinity of the nanopillars. The emission peaks formed along HNPs can be described as hotspots of radiate energy emitted from fluorophores due to plasmonic coupling of the gold caps at the tips of HNPs with localized plasmon modes. The normalized intensity of the fluorescence emission peaks was approximately 300 times that of the peripheral part. We found that the emission spots from fluorophores on HNPs were 25-fold brighter than those from fluorophores on DNPs. Then, we measured the FWHM profiles of the fluorescence distributions of HNPs against those of DNPs to investigate the enhancement of hybrid plasmonic modes (Figure 3d). The FWHM of the HNPs was measured in the entire area except for the nucleus. The average FWHM value of the fluorescence peak for HNPs was approximately 210 nm, which approximated

the expected volume of photonic-plasmonic waveguide-based illumination based on the previous simulations.

Based on the above results, we observed that the illumination area of the fluorescent targets was determined by the plasmon field zone from surface of the gold nanodisks. This area represents the nanoscale detection volume; thus, we expect that HNPs can be observed even if the size of the target material is smaller than 10 nm.

2.4 Plasmonic-supported fluorescence imaging of intracellular and intranuclear EGF with enhanced spatial resolution for two-photon illumination

To verify the high-resolution 3D imaging performance of HNP platforms, we conducted experimental tests to detect two-photon excited fluorescence coupled with the metallic cap of HNPs and single biomolecules acting inside the nucleus of cells cultured on HNPs by Two-photon microscopy (TPM) (Figure 4a). In this section, we verify the improvement in the lateral resolution in
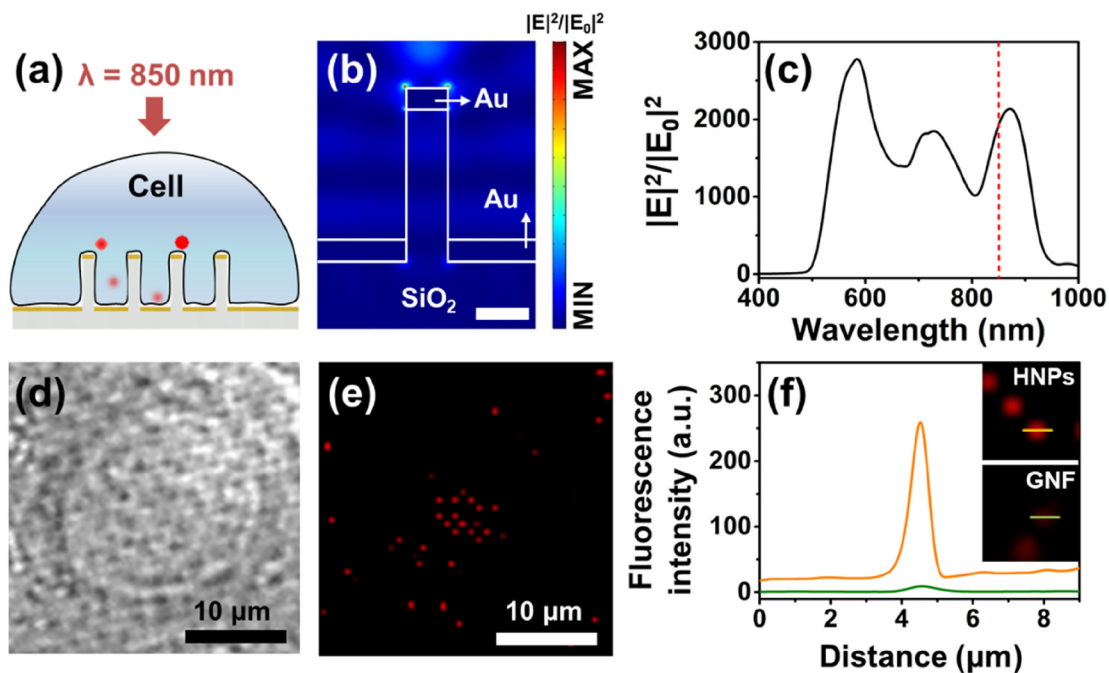
Figure 4: Two-photon excitation of HNPs within living cells for investigating the capability for high-resolution detection of EGFs transported in the nucleus. (a) Schematic illustration of the two-photon excited fluorescence concentration of intracellular epidermal growth factor (EGF) treated with Alexa 647 coupled with gold caps of HNPs. (b) Calculated near-field intensity distribution of HNPs under 850 nm laser illumination (scale bar: 200 nm). (c) Simulated intensity enhancement over the wavelength range from 400 to 1000 nm at the gold cap of HNPs to confirm the validity of plasmonic focusing generation for two-photon excitation. (d) Bright field images of HeLa cells cultured on HNPs. (e) Fluorescent visualization of intranuclear EGF-attached Alexa 647 (red channel) in HeLa cells. (f) Comparison of the fluorescence signal intensities of EGF molecules under the interaction with the gold cap of HNPs and on a GNF.

advance by demonstrating fluorescence enhancement and via quantitative analysis of the resolution of fluorescence signals excited with plasmon focussing of the HNPs.

We selected EGF, which transduces its actions via the EGF receptor and can be trafficked from the plasma membrane to either the cytoplasm or the nucleus. Through additional simulations, we confirmed that HNPs were suitable for use as detecting probes with plasmonic focussing at the gold caps in the TPM system used in the study (Figure 4b). We matched the resonance wavelength of the gold cap and the excitation wavelength of the two-phonon fluorescence system based on the result of the simulation to find the appropriate excitation wavelength (Figure 4c). Regarding the previously mentioned issue in Figure S6, additional simulations were performed under the conditions adapted in TPM system (ESI Figure S7). We could confirm that the direction and wavelength of the incident light which is TPM system condition and the surface uniformity insignificantly affect the generation of plasmonic hotspots at the edge of Au cap.

In sequence, we obtained HNP-mediated EGF fluorescence images at 700 nm in height, which correspond to the inside of the cell nucleus. EGF fluorescence signals were formed, appearing as a pixel array, according to the nanopillar pattern because the plasmonic caps of HNPs generated improved localization of fluorescence emission (Figure 4e). Then, we investigated the enhanced fluorescence signal of EGF molecules in the cell nucleus due to the coupling between the fluorophore and gold nanocap of HNPs based on two-photon measurements. We found that the local field enhancement near the metal nanocap for an appropriate proximity of the fluorophores to the gold nanodisks of HNPs led to greatly enhanced fluorescence emission (Figure 4f). The observed TPEF on the gold patterned surface was enhanced by over 34 orders of magnitude compared to that of the molecules on a GNF surface. The measured FWHM of the fluorescence signals coupled with HNPs was approximately 190 nm, similar to the diameter of the gold caps of HNPs. These phenomena were expected to enhance the lateral resolution via coupling of plasmonic hotspots, as in the previously conducted simulations.

The cell nucleus serves as an expression supporter of various biomolecules internalized from the extracellular membrane through endocytosis. Analysis of the activity and mechanism of these molecules is critical to demonstrate the interaction of the nucleus and the single EGF molecules transported into the nucleus because these biomolecules can sensitively affect cell division and cellular cycles and work in detail.

2.5 Axial super-resolved imaging of EGF behaviour at the plasmonic cap by plasmon-enhanced two-photon fluorescence microscopy

To evaluate the enhancement of axial resolution performance in HNPs, we experimentally verified the characteristics of the intensity point spread function from individual EGF signals in the axial direction on 3D reconstructed images obtained via plasmonic-assisted TPM. Figure 5a displays 3D fluorescence images of fluorescent molecules attached to EGF transported inside cells cultured on GNF and HNPs, which were scanned at intervals of 100 nm along the z-axis, displaying additional XY and XZ cross-sectional planes. When comparing the XY-plane images measured on GNF and HNPs, we found that the fluorescence signals were weak and blurred on the GNF substrate, but strong and sub-diffraction-limited excitation spots of EGF were detected on HNPs. The lateral resolution was improved by the plasmon focussing effect of HNPs leading to concentration of emitted fluorescence signals. And then, the XZ-plane images of the 3D image demonstrate show how much the HNP-assisted imaging technology enhances the axial resolution (Figure 5b). Fluorescent molecules conjugated to EGF on GNF substrates were measured as being stretched along the axial Z direction, with relatively low intensity and reduced imaging contrast. We also observed an aggregation-induced response on GNF, which led to failure in resolving the fluorescent objects. However, the 3D images observed on HNPs indicate that HNPs can enable almost conclusive acquisition of separated fluorescent hotspots with improved axial position detection. In HNP-assisted TPM, localized EGF fluorescence signals can be detected that allow single-molecule detection with improved axial resolution (Figure 5b).

We quantified the fluorescence intensity from each EGF signal measured through a series of Z-stack images detected on GNF and HNP substrates and display a scatter plot of the fluorescence intensity distribution along the Z-axis direction, derived from the 95% confidence ellipse (Figure 5c). The plasmonic cap effect resulted in an amplified fluorescence intensity by a factor of ~60. These results provide a stringent comparison of the frequency distributions of the fluorescence intensity in the gold films and HNPs, which indicate an enhanced sensitivity of detecting each important signal with a high resolution based on the response expected in the previous simulation. The distribution was consistent for stronger field intensities, and the HNP technique has superb efficiency in plasmonic coupling of the gold caps of HNPs.

As shown in Figure 5d, we measured the intensity profiles and calculated the FWHM linewidth, which was
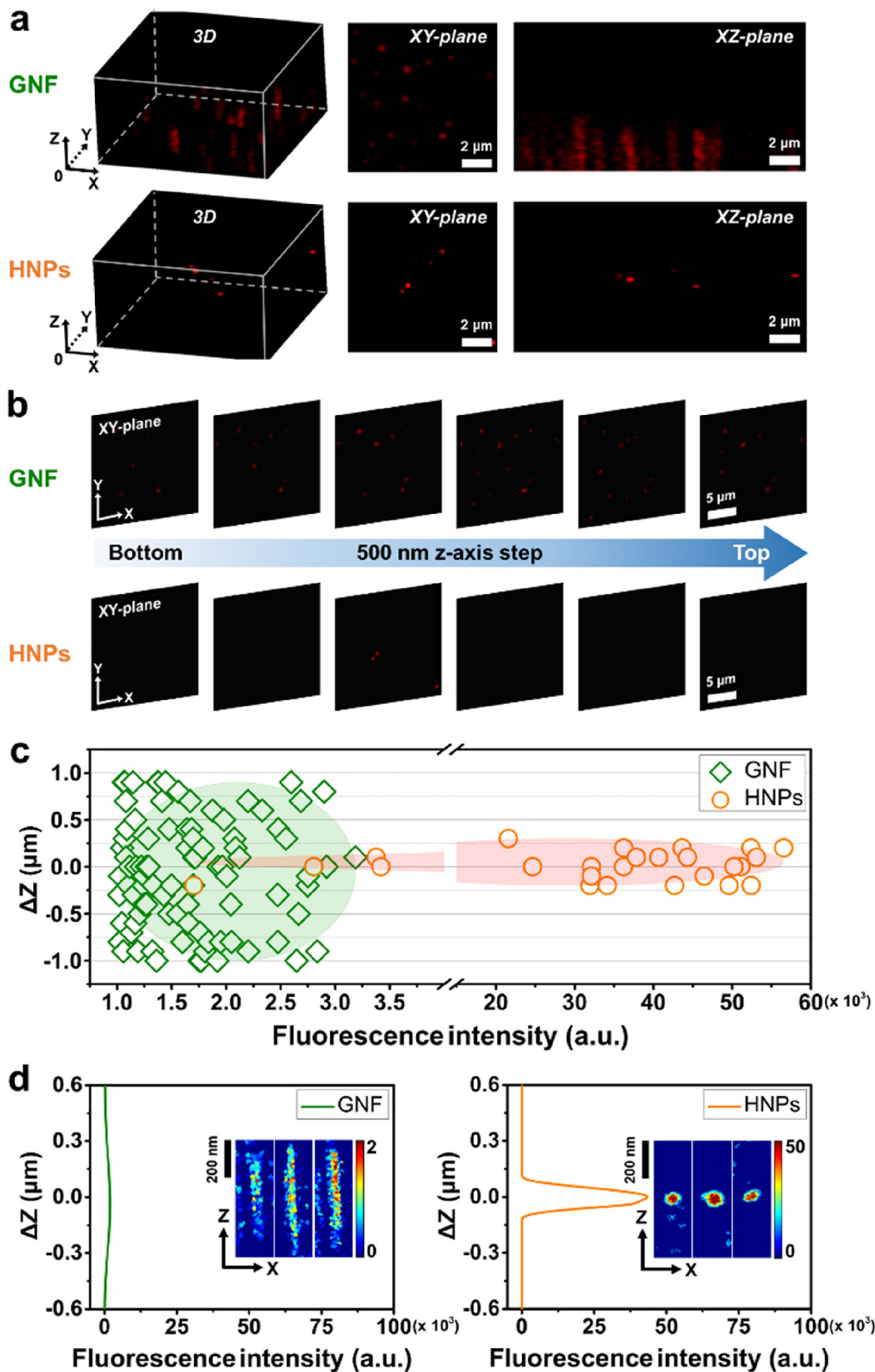
Figure 5: Analysis of axial resolution performance using HNP-based fluorescence emission in a two-photon optical system. (a) Representative 3D visualization of EGF signals on gold films and HNPs obtained via TPM. (b) Vertical cross-section of EGF signals on the GNF and HNPs at different z-positions. (c) Fluorescence intensity distribution of EGF signals emitted on gold films and HNPs in 3D images. (d) Intensity plots fitted to a Gaussian curve for estimation of the depth resolution of single fluorescent molecules with a nanoscale size, measured on HNPs and GNF.

used as the resolution criterion, of each emission peak intensity value in the 3D images observed on gold films and HNPs. The FWHM of plasmon-based fluorescence emission was 110 nm smaller than the observation volume under a conventional multiphoton microscope, whereas the FWHM of EGF signals was 556 nm on the gold films. HNP-based fluorescence imaging was proven to provide a dramatic axial resolution enhancement and has great potential for use in 3D tracking of various proteins in heterogeneous intracellular and nuclear environments. Consequently, the performance of fluorescence microscopy based on HNPs exhibits a significantly improved detection efficiency that achieves simultaneous enhancements in the fluorescence intensity and imaging resolution of single molecules.

Most high-resolution techniques, such as plasmonic 2D structures and photonic waveguide methods, have been used to observe many significant molecular events near membranes [13–53]. However, it is usually difficult to measure biomolecules in the vicinity of the nucleus. High-resolution imaging with a reasonable fluorescence enhancement is certainly required in the complex environment at the nucleus because single molecules are usually smaller in size than the light wavelength. Utilization of a plasmonic structure that can increase the fluorescence intensity at the nanoscale as a detection probe focused on the cellular nucleus is an outstanding technique. Of course, the technique with HNPs cannot reveal the overall cell behaviours or multiple-cell interactions due to the limitation on the positioning of the nanostructures. However, we expect that our proposal can provide a definite method to find very specific and targeted events inside a single cell at a given depth. These structures will provide exceptional ways to study the single-molecule reactions and mechanisms inside the cell nucleus.

3 Conclusion

We have developed a straightforward method using HNPs to effectively probe and instrumentally characterize intranuclear individual molecules. The plasmonic caps on the proposed HNPs provide improved functionality to produce strong interactions between the target molecules and localized plasmon-enhanced field. This phenomenon was predicted and characterized based on the near-field distribution around HNPs, creating light localization according to wave-optical simulations, followed by experimental investigations of cell–HNP adhesion and localized plasmon-based probing of living cells. The plasmon-based fluorescence amplification process was demonstrated in conventional fluorescence detection with linear optical

properties and nonlinear two-photon illumination. In conventional linear fluorescence imaging of HNPs, the enhancement factor of the fluorescence intensity was 25 and the lateral FWHM was 210 nm, compared with the value of 556 nm measured on DNPs. With the TPM imaging system, a 34-fold enhancement factor in the fluorescence of the EGF molecules measured on HNPs compared with GNF was achieved, and an improved resolution of 189 nm in the lateral dimension and 110 nm in the axial dimension of each EGF molecule signal was achieved. we simultaneously improved the lateral and axial resolutions below the diffraction limit using only HNPs without modification of the microscope system. Consequently, these novel and versatile HNP structures have great potential to clearly measure accurate position information, even in environments with aggregation of biotargets and imaging systems that have detection limits of fluorescence emission and optical 3D measurement.

4 Materials and methods

4.1 Fabrication of the HNPs

DNP and HNP arrays were fabricated using e-beam lithography and reactive ion etching technology (ESI Figure S1). Poly(methyl 2-methylpropenoate) (PMMA) (Allresist GmbH, AR-P 672.045) and a conducting polymer (Allresist GmbH, AR-PC 5090.02) were sequentially coated on a quartz substrate with a 1-mm thickness and a 1×1 cm^2 area at 1000 rpm for 90 s and 4000 rpm for 60 s, respectively. After that, they were baked for 4 and 3 min at 165 and 95 °C, respectively. Hole arrays with a diameter of 200 nm and a period of 1 μm were patterned on the PMMA layer using e-beam lithography. A Cr nanolayer with a 50 nm thickness was deposited using an e-beam evaporator, followed by a lift-off process to create Cr nanodisks that functioned as an etching mask to protect the geometry of the nanopillars from the etch plasma. Ar (7 sccm) and CF4 (5 sccm) gases were simultaneously incident on the Cr nanodisks on the quartz substrate by etching for 3 h at 50 W. The arranged SiO_2 nanopillar arrays were approximately 200 nm in diameter and 700 nm in height with a 1 μm period in a cylindrical shape. To fabricate HNP arrays, we sequentially deposited a 5 nm Cr layer and a 100 nm Au layer on DNP arrays via e-beam and thermal evaporation methods, respectively. The substrate was sterilized in ethanol and coated for 5 min with a 0.1% poly-L-lysine solution, followed by aspiration of the solution and sterilization under UV light for 30 min. To investigate distinct separation of Au and SiO_2, the energy dispersive X-ray spectrum images of HNPs were acquired with a field-emission scanning electron microscope (FE-SEM, ZEISS SUPRA 40 VP) equipped with an Oxford energy-dispersive X-ray spectrometer (EDX).

4.2 Simulations and structural design

A simulation was carried out to confirm the pattern and electric field distribution of the plasmonic hotspots of the HNPs

proposed in this study using a finite element method. The basic structure used in the simulation was a circular DNP with a diameter of 200 nm, a height of 700 nm, and a period of 1000 nm, which set based on the results of previous studies [18, 19] for optimal cell-nanopillar interaction conditions. The HNPs was designed DNPs with the addition of gold nanolayer of 100 nm in height at the tips and substrate of the nanopillars, the same size as a fabricated nanopillar (ESI Figure S2). The materials of the substrate below the nanopillar and of the nanopillar were set to SiO_2. The set constants of SiO_2 and gold came from Malitson and Rakic, respectively. The surrounding medium of the nanopillar was set to water (n = 1.33). The wavelength of the incident light was 633 nm, the polarization mode was transverse magnetic, and the power was 1 W. The incident light approached the nanopillar along the axis of the nanopillar. To obtain accurate results, we added a perfectly matched layer to prevent electromagnetic waves from scattering within a limited physical space outside of the physical space.

4.3 Cell culture and fluorescence treatment

HeLa epithelial cells were obtained from the American Type Culture Collection. The fabricated nanoantenna substrates were sterilized by rinsing with 100% ethanol and dried under UV light for 30 min. Following nanostructure sterilization, HeLa cells were cultured on the substrates in Dulbecco's modified Eagle medium (Gibco™, 10569010) supplemented with 10% fetal bovine serum (Gibco™, 16000036) and 1% gentamicin (Gibco™, 15750060) in an incubator at 37 °C under 5% CO2 and 95% humidity for 24 h. The cell adhesion of the nanoantenna array was analysed by SEM. We selected fluorescent dyes to excite and detect fluorophores in the cell membrane and nuclei labelled with DiD (AAT Bioquest, 22,033, USA) and T-PRO-3 iodide (Invitrogen™, T3605, Ireland) labelling solutions, respectively. They were red-emitting fluorescent dyes that enable excitation at 632.8 nm and were prepared in 5 and 20 μM working solutions in dimethyl sulfoxide, respectively. HeLa cells grown on DNPs and HNPs in the culture medium were treated with DiD and T-PRO-3 iodide labelling solutions at 37 °C for 5 and 15 min, respectively. After the treatment, the labelled cells cultured on probe substrates were washed with prewarmed growth medium. To measure the fluorophore signal from biomolecular movement inside the cell nucleus, we selected EGF, which is a biological molecule that can be internalized and transported deep within cells as an endosomal compartment of the EGF receptor–ligand complex by clathrin-mediated endocytosis. HeLa cells were grown on HNP arrays in the culture medium to reach 70% confluence on the day of the experiment and were washed three times with PBS, followed by treatment with 200 ng/mL EGF complex stained with Alexa Fluor 647 (red) in Dulbecco's modified Eagle medium at 37 °C for 30 min. The cells were washed four times with cold PBS to remove EGF on areas apart from the cells.

4.4 SEM sample preparation

Cell adhesion analysis of the HNP array was investigated by SEM. For SEM, cells were fixed in a 2.5% glutaraldehyde solution (Sigma-Aldrich, G7526) in PBS at 4 °C and rinsed for 1 h. Next, the cells were dehydrated by ethanol solutions with gradually increasing concentrations from 50 to 100% in sterilized water and dried at room temperature for 1 h. Before SEM, the cells were sputtered with a few nanometre of gold.

4.5 Optical setup of one-photon fluorescence imaging

A wavelength of 632.8 nm, an initial intensity of 21 mW, and a plane wave laser were used (Thorlabs, HNL210L) (ESI Figure S3). A lens was added to increase the beam size. The beam travelled perpendicular to the sample, passed through the lens, and was focused on the sample. The fluorescence from the sample was collected with a 100x, NA 0.9 objective lens (Olympus, MPlanFL N). The central wavelength was 660 nm (±5 nm), and the excitation filter (Edmund Optics, 87,755) with 94% transmission only transmitted fluorescence into the camera equipment (Thorlabs, DCU223C).

4.6 Optical setup of multiphoton fluorescence imaging

TPM is an excellent nanoscopic imaging technology based on nonlinear excitation. Thus, high-resolution three-dimensional (3D) images of biological materials in complex environments can be obtained, whereby this approach is useful for investigating the morphology and dynamics information of cells. In particular, the TPM technique is useful for measuring the fluorescence signals of cells cultured on nanostructures, such as the high-aspect-ratio nanopillars proposed in this study. A wavelength-tunable Ti:sapphire femtosecond ultrashort pulse laser (wavelength 680–1080 nm, pulse duration 140 fs, repetition rate 80 MHz) was used for the TPM laser source (ESI Figure S4). We selected an 850 nm wavelength to improve the excitation efficiency of the Alexa 647 fluorophores (Em 647 nm, Ex 665 nm) labelling EGF. Then, the average power of the laser was optimized for efficient measurement of the nonlinear fluorescence signals from the sample cells without cellular damage. Because the Ti:sapphire laser has a horizontal linearly polarized output, the average power of the laser could be adjusted with a half-wave plate and a linear polarizer. Then, the laser was circularly polarized using a quarter-wave plate and extended by an optical beam expander to fill the back aperture of the objective lens. The extended beam was focused on the sample through an oil-immersion objective lens with a magnification of 40x and a numerical aperture of 1.4. The two photon-induced fluorescence signals, produced by the tightly focused beam, were collected through the same objective lens and then directed to a longpass dichroic mirror set with three colour channels (red, green, and blue). The separated three-colour fluorescence signals were filtered by bandpass filters and then detected by photomultiplier tubes (H10682-210, Hamamatsu Photonics). Two-dimensional (2D) images were obtained through dual-axis (x, y) raster scanning using two galvanometers, and 3D rendered images were obtained through processing of several images collected at different focal planes using a motorized microscope stage along the z direction.

References

[1] Z. Liu, L. D. Lavis, and E. Betzig, "Imaging live-cell dynamics and structure at the single-molecule level," *Mol. Cell*, vol. 58, no. 4, pp. 644–659, 2015, https://doi.org/10.1016/j.molcel.2015.02.033.

[2] T. Kues, R. Peters, and U. Kubitscheck, "Visualization and tracking of single protein molecules in the cell nucleus," *Biophys. J.*, vol. 80, no. 6, pp. 2954–2967, 2001, https://doi.org/10.1016/s0006-3495(01)76261-3.

[3] A. C. De Angelis Campos, M. A. Rodrigues, C. de Andrade, A. M. de Goes, M. H. Nathanson, and D. A. Gomes, "Epidermal growth factor receptors destined for the nucleus are internalized via a clathrin-dependent pathway," *Biochem. Biophys. Res. Commun.*, vol. 412, no. 2, pp. 341–346, 2011, https://doi.org/10.1016/j.bbrc.2011.07.100.

[4] T. M. Brand, M. Iida, C. Li, and D. L. Wheeler, "The nuclear epidermal growth factor receptor signaling network and its role in cancer," *Discov. Med.*, vol. 12, no. 66, p. 419, 2011.

[5] J. P. Siebrasse, T. Kaminski, and U. Kubitscheck, "Nuclear export of single native mrna molecules observed by light sheet fluorescence microscopy," *Proc. Natl. Acad. Sci. U.S.A.*, vol. 109, no. 24, pp. 9426–9431, 2012, https://doi.org/10.1073/pnas.1201781109.

[6] C. I. Richards, K. Luong, R. Srinivasan, et al., "Live-Cell imaging of single receptor composition using zero-mode waveguide nanostructures," *Nano Lett.*, vol. 12, no. 7, pp. 3690–3694, 2012, https://doi.org/10.1021/nl301480h.

[7] T. Miyake, T. Tanii, H. Sonobe, et al., "Real-time imaging of single-molecule fluorescence with a zero-mode waveguide for the analysis of protein– protein interaction," *Anal. Chem.*, vol. 80, no. 15, pp. 6018–6022, 2008, https://doi.org/10.1021/ac800726g.

[8] J. Ma and W. Yang, "Three-dimensional distribution of transient interactions in the nuclear pore complex obtained from single-molecule snapshots," *Proc. Nat. Acad. Sci. U S A*, vol. 107, no. 16, pp. 7305–7310, 2010, https://doi.org/10.1073/pnas.0908269107.

[9] J. Zhang, Y. Fu, and J. R. Lakowicz, "Single cell fluorescence imaging using metal plasmon-coupled probe," *Bioconjug. Chem.*, vol. 18, no. 3, pp. 800–805, 2007, https://doi.org/10.1021/bc0603384.

[10] A. Kinkhabwala, Z. Yu, S. Fan, Y. Avlasevich, K. Müllen, and W. E. Moerner, "Large single-molecule fluorescence enhancements produced by a bowtie nanoantenna," *Nat. Photon.*, vol. 3, no. 11, pp. 654–657, 2009, https://doi.org/10.1038/nphoton.2009.187.

[11] J. M. Moran-Mirabal, A. J. Torres, K. T. Samiee, B. A. Baird, and H. G. Craighead, "Cell investigation of nanostructures: zero-mode waveguides for plasma membrane studies with single molecule resolution," *Nanotechnology*, vol. 18, no. 19, 2007, https://doi.org/10.1088/0957-4484/18/19/195101.

[12] E. Arbabi, J. Li, R. J. Hutchins, et al., "Two-photon microscopy with a double-wavelength metasurface objective lens," *Nano Lett*, vol. 18, no. 8, pp. 4943–4948, 2018, https://doi.org/10.1021/acs.nanolett.8b01737.

[13] C. Xie, L. Hanson, Y. Cui, and B. Cui, "Vertical nanopillars for highly localized fluorescence imaging," *Proc. Nat. Acad. Sci. U.S.A.*, vol. 108, no. 10, pp. 3894–3899, 2011, https://doi.org/10.1073/pnas.1015589108.

[14] R. S. Frederiksen, E. Alarcon-Llado, P. Krogstrup, et al., "Nanowire-aperture probe: local enhanced fluorescence detection for the investigation of live cells at the nanoscale," *ACS Photon.*, vol. 3, no. 7, pp. 1208–1216, 2016, https://doi.org/10.1021/acsphotonics.6b00126.

[15] M. Kandziolka, J. J. Charlton, I. I. Kravchenko, et al., "Silicon nanopillars as a platform for enhanced fluorescence analysis," *Anal. Chem.*, vol. 85, no. 19, pp. 9031–9038, 2013, https://doi.org/10.1021/ac401500y.

[16] K. Sengupta, E. Moyen, and M. Mace, "Large-scale ordered plastic nanopillars for quantitative live-cell imaging," *Small*, vol. 5, no. 4, pp. 449–453, 2009, https://doi.org/10.1002/smll.200800836.

[17] A. K. Shalek; J. T. Robinson, E. S. Karp, et al., "Vertical silicon nanowires as a universal platform for delivering biomolecules into living cells," *Proc. Nat. Acad. Sci. U.S.A.*, vol. 107, no. 5, pp. 1870–1875, 2010, https://doi.org/10.1073/pnas.0909350107.

[18] F. Santoro, W. Zhao, L.-M. Joubert, et al., "Revealing the cell–material interface with nanometer resolution by focused ion beam/scanning electron microscopy," *ACS Nano.*, vol. 11, no. 8, pp. 8320–8328, 2017, https://doi.org/10.1021/acsnano.7b03494.

[19] L. Hanson, W. Zhao, H. Y. Lou, et al., "Vertical nanopillars for in situ probing of nuclear mechanics in adherent cells," *Nat. Nanotechnol.*, vol. 10, no. 6, pp. 554–562, 2015, https://doi.org/10.1038/nnano.2015.88.

[20] F. Mumm, K. M. Beckwith, S. Bonde, K. L. Martinez, and P. Sikorski, "A transparent nanowire-based cell impalement device suitable for detailed cell-nanowire interaction studies," *Small*, vol. 9, no. 2, pp. 263–272, 2013, https://doi.org/10.1002/smll.201201314.

[21] C. Y. Tay, S. A. Irvine, F. Y. Boey, L. P. Tan, and S. Venkatraman, "Micro-/nano-engineered cellular responses for soft tissue engineering and biomedical applications," *Small*, vol. 7, no. 10, pp. 1361–1378, 2011, https://doi.org/10.1002/smll.201100046.

[22] W. Kim, J. K. Ng, M. E. Kunitake, B. R. Conklin, and P. Yang, "Interfacing silicon nanowires with mammalian cells," *J. Am. Chem. Soc.*, vol. 129, no. 23, pp. 7228–7229, 2007, https://doi.org/10.1021/ja071456k.

[23] S. Qi, C. Yi, S. Ji, C. C. Fong, and M. Yang, "Cell adhesion and spreading behavior on vertically aligned silicon nanowire arrays," *ACS Appl. Mater. Interfaces*, vol. 1, no. 1, pp. 30–34, 2008, https://doi.org/10.1021/am800027d.

[24] D. Liu, C. Yi, K. Wang, et al., "Reorganization of cytoskeleton and transient activation of ca2+ channels in mesenchymal stem cells cultured on silicon nanowire arrays," *ACS Appl. Mater. Interfaces*, vol. 5, no. 24, pp. 13295–13304, 2013, https://doi.org/10.1021/am404276r.

[25] W. Hällström, T. Mårtensson, C. Prinz, et al., "Gallium phosphide nanowires as a substrate for cultured neurons," *Nano Lett.*, vol. 7, no. 10, pp. 2960–2965. 2007, https://doi.org/10.1021/nl070728e.

[26] H. R. Seo, H. J. Joo, D. H. Kim, et al., "Nanopillar surface topology promotes cardiomyocyte differentiation through cofilin-mediated cytoskeleton rearrangement," *ACS Appl. Mater. Interfaces*, vol. 9, no. 20, pp. 16803–16812, 2017, https://doi.org/10.1021/acsami.7b01555.

[27] J. M. Lopacinska, C. Gradinaru, R. Wierzbicki, et al., "Cell motility, morphology, viability and proliferation in response to

nanotopography on silicon black," *Nanoscale*, vol. 4, no. 12, pp. 3739–3745, 2012, https://doi.org/10.1039/c2nr11455k.

[28] H. Persson, C. Kobler, K. Molhave, et al., "Fibroblasts cultured on nanowires exhibit low motility, impaired cell division, and dna damage," *Small*, vol. 9, no. 23, pp. 4006–4016, 2013, Art no. 3905, https://doi.org/10.1002/smll.201300644.

[29] X. Guo, Y. Ying, and L. Tong, "Photonic nanowires: from subwavelength waveguides to optical sensors," *Acc. Chem. Res.*, vol. 47, no. 2, pp. 656–666, 2013, https://doi.org/10.1021/acsphotonics.5b00112.

[30] D. R. Abujetas, R. Paniagua-Domínguez, and J. A. Sánchez-Gil, "Unraveling the janus role of mie resonances and leaky/guided modes in semiconductor nanowire absorption for enhanced light harvesting," *ACS Photon.*, vol. 2, no. 7, pp. 921–929, 2015, https://doi.org/10.1021/acsphotonics.5b00112.

[31] D. Verardo, F. W. Lindberg, N. Anttu, et al., "Nanowires for biosensing: lightguiding of fluorescence as a function of diameter and wavelength," *Nano Lett.*, vol. 18, no. 8, pp. 4796–4802, 2018, https://doi.org/10.1021/acs.nanolett.8b01360.

[32] R. Frederiksen, G. Tutuncuoglu, F. Matteini, K. L. Martinez, I. M. A. Fontcuberta, and E. Alarcon-Llado, "Visual understanding of light absorption and waveguiding in standing nanowires with 3d fluorescence confocal microscopy," *ACS Photon.*, vol. 4, no. 9, pp. 2235–2241, 2017, https://doi.org/10.1021/acsphotonics.7b00434.s001.

[33] D. K. Gramotnev and S. I. Bozhevolnyi, "Plasmonics beyond the diffraction limit," *Nat. Photon.*, vol. 4, no. 2, pp. 83–91, 2010, https://doi.org/10.1038/nphoton.2009.282.

[34] J. D. Caldwell, O. Glembocki, F. J. Bezares, et al., "Plasmonic nanopillar arrays for large-area, high-enhancement surface-enhanced raman scattering sensors," *ACS Nano.*, vol. 5, no. 5, pp. 4046–4055, 2011, https://doi.org/10.1021/nn200636t.

[35] C. Wang, M. Hossain, L. Ma, Z. Ma, J. J. Hickman, and M. Su, "Highly sensitive thermal detection of thrombin using aptamer-functionalized phase change nanoparticles," *Biosens. Bioelectron*, vol. 26, no. 2, pp. 437–443, 2010, https://doi.org/10.1016/j.bios.2010.07.097.

[36] P. Ponzellini, X. Zambrana-Puyalto, N. Maccaferri, L. Lanzanò, F. De Angelis, and D. Garoli, "Plasmonic zero mode waveguide for highly confined and enhanced fluorescence emission," *Nanoscale*, vol. 10, no. 36, pp. 17362–17369, 2018, https://doi.org/10.1039/c8nr04103b.

[37] Y. Fu and J. R. Lakowicz, "Enhanced fluorescence of cy5-labeled oligonucleotides near silver island films: a distance effect study using single molecule spectroscopy," *J. Phys. Chem. B*, vol. 110, no. 45, pp. 22557–22562, 2006, https://doi.org/10.1021/jp060402e.s001.

[38] R. L. Agapov, B. Srijanto, C. Fowler, D. Briggs, N. V. Lavrik, and M. J. Sepaniak, "Lithography-free approach to highly efficient, scalable sers substrates based on disordered clusters of disc-on-pillar structures," *Nanotechnology*, vol. 24, no. 50, pp. 505302, 2013, https://doi.org/10.1088/0957-4484/24/50/505302.

[39] A. Polemi, S. M. Wells, N. V. Lavrik, M. J. Sepaniak, and K. L. Shuford, "Local field enhancement of pillar nanosurfaces for SERS," *J. Phys. Chem. C*, vol. 114, no. 42, pp. 18096–18102, 2010, https://doi.org/10.1021/jp106540q.

[40] S. M. Wells, A. Polemi, N. V Lavrik, K. L. Shuford, and M. J. Sepaniak, "Efficient disc on pillar substrates for surface enhanced raman spectroscopy," *Chem. Commun.*, vol. 47, no. 13, pp. 3814–3816, 2011, https://doi.org/10.1039/c0cc05577h.

[41] W. Kubo and S. Fujikawa, "Au double nanopillars with nanogap for plasmonic sensor," *Nano Lett.*, vol. 11, no. 1, pp. 8–15, 2011, https://doi.org/10.1021/nl100787b.

[42] S. Kuhn, U. Hakanson, L. Rogobete, and V. Sandoghdar, "Enhancement of single-molecule fluorescence using a gold nanoparticle as an optical nanoantenna," *Phys. Rev. Lett.*, vol. 97, no. 1, 2006, Art no. 17402, https://doi.org/10.1103/physrevlett.97.017402.

[43] Y. Tuna, J. T. Kim, H. W. Liu, and V. Sandoghdar, "Levitated plasmonic nanoantennas in an aqueous environment," *ACS Nano.*, vol. 11, no. 8, pp. 7674–7678, 2017, https://doi.org/10.1021/acsnano.7b03310.

[44] K. Wang, E. Schonbrun, P. Steinvurzel, and K. B. Crozier, "Scannable plasmonic trapping using a gold stripe," *Nano Lett.*, vol. 10, no. 9, pp. 3506–3511, 2010, https://doi.org/10.1021/nl101653n.

[45] J. A. Schuller, E. S. Barnard, W. Cai, Y. C. Jun, J. S. White, and M. L. Brongersma, "Plasmonics for extreme light concentration and manipulation," *Nat. Mater.*, vol. 9, no. 3, pp. 193–204, 2010, https://doi.org/10.1038/nmat2630.

[46] A. McLintock, H. J. Lee, and A. W. Wark, "Stabilized gold nanorod-dye conjugates with controlled resonance coupling create bright surface-enhanced resonance raman nanotags," *Phys. Chem. Chem. Phys.*, vol. 15, no. 43, pp. 18835–18843, 2013, https://doi.org/10.1039/c3cp52946k.

[47] G. P. Acuna, F. M. Möller, P. Holzmeister, S. Beater, B. Lalkens, and P. Tinnefeld, "Fluorescence enhancement at docking sites of dna-directed self-assembled nanoantennas," *Science*, vol. 338, no. 6106, pp. 506–510. 2012, https://doi.org/10.1126/science.1228638.

[48] J. E. Donohue, E. Wertz, C. N. Talicska, and J. S. Biteen, "Plasmon-enhanced brightness and photostability from single fluorescent proteins coupled to gold nanorods," *J. Phys. Chem. C*, vol. 118, no. 27, pp. 15027–15035, 2014, https://doi.org/10.1021/jp504186n.

[49] S. Y. Liu, L. Huang, J. F. Li, et al., "Simultaneous excitation and emission enhancement of fluorescence assisted by double plasmon modes of gold nanorods," *J. Phys. Chem. C*, vol. 117, no. 20, pp. 10636–10642, 2013, https://doi.org/10.1021/jp4001626.

[50] M. H. Chowdhury, K. Ray, K. Aslan, J. R. Lakowicz, and C. D. Geddes, "Metal-enhanced fluorescence of phycobiliproteins from heterogeneous plasmonic nanostructures," *J. Phys. Chem. C Nanomater. Interfaces*, vol. 111, no. 51, pp. 18856–18863, 2007, https://doi.org/10.1021/jp0731250.

[51] D. Punj, P. Ghenuche, and S. B. Moparthi, et al., "Plasmonic antennas and zero-mode waveguides to enhance single molecule fluorescence detection and fluorescence correlation spectroscopy toward physiological concentrations," *Wiley Interdisc. Rev. Nanomed. Nanobiotechnol.*, vol. 6, no. 3, pp. 268–282, 2014, https://doi.org/10.1002/wnan.1261.

[52] D. Radziuk and H. Moehwald, "Prospects for plasmonic hot spots in single molecule sers towards the chemical imaging of live cells," *Phys. Chem. Chem. Phys.*, vol. 17, no. 33, pp. 21072–21093, 2015, https://doi.org/10.1039/c4cp04946b.

[53] A. B. Taylor and P. Zijlstra, "Single-molecule plasmon sensing: current status and future prospects," *ACS Sens.*, vol. 2, no. 8, pp. 1103–1122, 2017, https://doi.org/10.1021/acssensors.7b00382.

[54] L. Zhou, F. Ding, H. Chen, W. Ding, W. Zhang, and S. Y. Chou, "Enhancement of immunoassay's fluorescence and detection sensitivity using three-dimensional plasmonic nano-antenna-dots array," *Anal. Chem.*, vol. 84, no. 10, pp. 4489–4495, 2012, https://doi.org/10.1021/ac3003215.

[55] A. E. Cetin, A. A. Yanik, C. Yilmaz, S. Somu, A. Busnaina, and H. Altug, "Monopole antenna arrays for optical trapping, spectroscopy, and sensing," *Appl. Phys. Lett.*, vol. 98, no. 11, 2011, Art no. 111110, https://doi.org/10.1063/1.3559620.